FUNDAMENTAL LIMITATIONS TO THE OBSERVABILITY OF OUTSKIRTS OF (DWARF) GALAXIES AT HIGH REDSHIFTS:

THE NATURAL CONFUSION LIMIT IN ULTRADEEP OPTICAL–IR AND RADIO SURVEYS

Rogier A. Windhorst[1], Seth H. Cohen, Rolf A. Jansen, Stephen C. Odewahn

Department of Physics and Astronomy, Arizona State University, Tempe, AZ 85287-1504

{Rogier.Windhorst, Seth.Cohen, Rolf.Jansen, Stephen.Odewahn}@asu.edu

Simon P. Driver

Research School of Astronomy and Astrophysics, Australian National University, Cotter Road, Weston Creek, Canberra, ACT 2600, Australia

spd@mso.anu.edu.au

Daisuke Kawata, Brad K. Gibson

Centre for Astrophysics & Supercomputing, Swinburne University, Mail 31, P.O. Box 218, Hawthorn, Victoria, 3122, Australia

dkawata@astro.swin.edu.au, bgibson@astro.swin.edu.au

and

Andrew Hopkins

University of Pittsburgh, Department of Physics and Astronomy 3941 O'Hara Street, Pittsburgh, PA 15260

ahopkins@phyast.pitt.edu

Poster presented at the 2002 Lowell Observatory Workshop on "The Outer Edges of Dwarf Irregular Galaxies", Flagstaff, AZ. Paper to be submitted in two parts: to PASA and ApJ.

---

[1]Interdisciplinary Scientist for the James Webb Space Telescope (JWST)

1. ABSTRACT

We discuss the natural confusion limit in the red/near-IR for the 6.0 meter Next Generation Space Telescope (NGST) – now called the James Webb Space Telescope (JWST) and planned for launch to an L2 orbit in 2010 — and for the Square Kilometer Array (SKA) at radio wavelengths, that would become reality in the next decade. First, we summarize the observed half-light radius vs. magnitude relation for the entire galaxy population from the RC3 level to the HDF limit. Together with estimates of this relationship in hierarchical models at flux levels fainter than J(1.35 micron)$_{AB}$ $\simeq$28 mag and model extrapolations of the faint galaxy counts at J_{AB} $\simeq$28–34 mag, we estimate the natural confusion limit for JWST at 1.35 microns. At J_{AB} $\simeq$34 mag, the surface density of objects could be several tens of millions of objects per square degree, or several detected objects per square arcsecond.

A rather unexpected scientific result of this study is that in ultradeep surveys with $\simeq$0$''\!.$1 FWHM resolution, the natural confusion limit becomes *as* important in the definition of faint source samples as the traditional surface brightness (SB) limits. In particular, for resolutions of $\gtrsim$0$''\!.$08 FWHM, it appears that for J_{AB} $\gtrsim$25 mag (B $\gtrsim$27 mag) both HST and the JWST may be more affected by natural confusion than by the traditional SB-limits. We suggest that this may already be visible in the deepest HDF images. This does however not mean that the deepest JWST samples will be fundamentally limited by natural confusion. Instead, we expect that for J_{AB} $\gtrsim$28–30 mag, the faint objects seen by JWST will be largely point sources at 0$''\!.$08 FWHM, which we begin to address with hierarchical simulations. In this case, the deepest JWST images will be limited only by the instrumental confusion limit, which doesn't set in until around J_{AB} $\gtrsim$33.5 mag.

Having set constraints to the JWST natural confusion limit, it is relatively straightforward to calculate it for the SKA at GHz frequencies, since the same population of faint irregular, peculiar and merging/star-forming objects that dominates the faint galaxy counts will likely dominate the radio source counts at nanoJansky levels. For such objects, their radio sizes are likely similar to, or at least not much larger than their optical–IR sizes. If so, the SKA will need to have better than 50–100 m.a.s. FWHM in order to not run into the instrumental confusion limit at 100 nanoJy at 1.4 GHz. At levels of $S_{1.4}$ $\simeq$10 nanoJy, the SKA will reach similar object surface densities as the JWST at J_{AB} $\simeq$33 mag, and — like the JWST — not run into the natural confusion limit at $S_{1.4}$ $\simeq$10 nanoJy, *if* the slope of the nanoJy source counts remains below $\gamma\lesssim$1.7 (magnitude slope $\alpha\lesssim$0.28), and if the ratio of radio to optical–near-IR sizes remains close to unity at nanoJy levels.

Keywords: galaxies: high-redshift — galaxies: surveys — galaxies: dwarfs — instruments: James Webb Space Telescope — instruments: Square Kilometer Array

2. INTRODUCTION

In the last few decades, very significant efforts have been made on deep surveys of the sky, ranging from radio to infra-red to optical and X-ray wavelengths. In the optical–near-IR, for instance, the "faint blue galaxy" (FBG) population that dominates the faint galaxy counts (Kron 1980; Koo & Tyson 1988; Ellis 1997) has been shown by HST to consist predominantly of late-type, irregular and peculiar galaxies (e.g., Driver et al. 1995, 1998; Glazebrook et al. 1995; Abraham et al. 1996; Odewahn et al. 1996) which vastly outnumber the expected surface densities seen in local surveys (Driver et al. 1998, Marzke et al. 1998). At radio wavelengths, the sub-milliJansky population similarly showed a significant excess in surface densities over those expected from brighter levels (Windhorst et al. 1985, 1993), which a number of groups have shown (Kron et al. 1985, Benn et al. 1992, Hammer et al. 1995, Windhorst et al. 1995; Hopkins et al. 1999) is likely due to a mixture of star-forming and merging galaxies in addition to increased AGN activity in faint early-type galaxies at intermediate to high redshifts. The tentative conclusion from these optical-IR and radio surveys has been that we see the effects of the gradual hierarchical formation of galaxies and their central engines over Hubble time.

Given the rapidly preceding technology of both telescope design, correlators, detectors and data processing, telescopes are now under consideration or in the design phase that will reach nano-Jansky sensitivities at both radio and optical–near-IR wavelengths, i.e. a full factor of 100–1000 times more sensitive than what can be achieved with current state of the art technology (e.g., the VLA, HST). The telescope planned for the future are the 6.0 meter JWST (Mather & Stockman 2000, Stockman & Mather 2000) and the SKA (Hopkins et al. 2000; Ekers et al. 2000). A natural question to ask if whether the currently accomplished surveys show any evidence that the planned surveys at nano-Jansky levels will run into the natural confusion limit. This is not only an important question to ask before billions of dollars are spent on the final design and actual construction of these future telescopes, but also may provide insight in whether we can extend surveys fundamentally to arbitrarily faint levels, or whether we will run into fundamental limitations that will complicated such surveys or perhaps make them impossible to carry out. Related to this, it may help answer the question whether the usual survey properties such as point-source sensitivity and surface-brightness (SB) sensitivity are the only limiting factors to the new surveys expected in the next decade, or whether other fundamental issues will ultimately limit these surveys.

To begin answer these questions, we will in this paper first briefly review the classical instrumental confusion limit and the natural confusion limit (§3). Next, we summarize the available optical near-IR counts of galaxies and their distribution over half-light radii, covering the widest possible range in flux. From this we estimate in §4 the natural confusion limit as expected for the 6.0 m JWST. In §5, we will similarly review the available radio source counts and their angular size distribution over the widest possible range in flux, and from this we will derive the natural confusion limit expected for the SKA.

3. THE TWO CONFUSION LIMITS CLARIFIED

3.1. The Classical or Instrumental Confusion Limit

The classical instrumental confusion limit occurs when the sensitivity of a telescope is so good that the faint source surface density results in significant source overlap — typically at the rate of a deep survey having fewer than 50 independent instrumental beams or FWHM's per detected object (Condon 1974), depending somewhat on the slope of the faint objects counts following the P(D) analysis first introduced by Scheuer (1974). This effect hampers the construction of reliable and complete faint object samples and results in less reliable object catalogs (e.g., Bertin & Arnouts 1996).

3.2. The Natural Confusion Limit

The natural confusion limit occurs when the faint source population (with a median half-light radius r_e) is significantly resolved at the instrumental FWHM, *and* when their surface density is so high that one has fewer than a minimum number of "object beams" (with area $\pi \times r_e^2$) for each detected faint object. This is in essence based on the Rayleigh criterion, which requires objects to be $\gtrsim$FWHM/2 apart to be detected as separate.

4. THE NATURAL CONFUSION LIMIT FOR THE JAMES WEBB SPACE TELESCOPE

Here we address the natural confusion limit for the 6.0 meter James Webb Space Telescope (JWST), which is planned for launch to an L2 orbit in 2010 (Mather & Stockman 200; Im & Stockman 1999). The JWST will have all gold reflective optics and cover the wavelength range 0.6–30μm. It will be diffraction limited at $\lambda \geq$K-band (FWHM$\gtrsim 0.084''$). Its primary near-IR camera, NIRCam, will have very high-QE low-noise detectors, and yield nanoJy sensitivity at 0.6-5.3μm (Rieke et al. 2002). It will approximately reach J_{AB} $\simeq$31 mag at 10σ in 10-hrs, and it could reach J_{AB} $\simeq$33.5 mag in a dedicated 1000-hrs "super HDF-like" campaign (which may get done during JWST's life-time).

We estimate the faint galaxy counts at J_{AB} (1.35μm) $\simeq$28–35 mag from the models of Gardner (1998) and Gardner & Satyapal (2000), which basically are a smooth extrapolation of the counts as measured to AB$\simeq$30 mag with the HST HDF (WFPC2 and STIS), and include reasonable assumption about the LF and N(z) at fainter luminosities. Given the unknown role of faint dwarf galaxies, and perhaps new classes of objects not represented in these models, the model extrapolations to J_{AB} $\simeq$34 mag are at least uncertain in amplitude by 0.3 dex, which is however of little consequence in the argument that follows. In any case, at J_{AB} $\simeq$34 mag, we get 10–20$\times 10^6$ objects deg^2 , or several detected objects per square arcsecond! Needless to say this implies that one would approach the natural confusion limit if the object sizes were still a good fraction of an arcsecond.

To compute the natural confusion limit for the JWST, we first summarize the half-light radius vs. magnitude relation for the entire galaxy population from the RC3 level to the HDF limit. In Fig. 2 we plot the total B-magnitude versus effective or half-light radius r_e for the entire galaxy population, as available. Details are given in Cohen et al. (2002), Liske et al. (2001), and Odewahn et al. (1996, 2002). We estimate the natural confusion limit for JWST at 1.35 microns as following. From the observed slope of the galaxy counts (α $\simeq$0.3 for λ $\simeq$B$\rightarrow$K; Fig. 1 here, Maihara et al. 2001; Gardner et al. 2000) and the galaxy size distribution (Fig. 2–4), we predict the JWST *instrumental* confusion limit to occur at $J_{AB} \gtrsim 33.5$ mag, where the number of independent beams (with FWHM$\gtrsim$0$''\!.$084) per detected object falls below 50 (*i.e.*, the classical confusion limit). The JWST *natural* confusion limit is assumed to occur when the galaxy density exceeds the level where there are fewer than $50\times\pi\ r_e^2$ "independent galaxy beams" for each detected object, which depends on the galaxy counts and size distribution for AB$\gtrsim$29 mag. We estimate it from the above mentioned galaxy counts, and plot the resulting natural confusion limit as slanted pink lines in Fig. 3–4.

A rather unexpected scientific result of this study is that in ultradeep surveys, the natural confusion limit becomes *as* important in the definition of faint source samples as the traditional SB-limits. In particular, for resolutions of $\gtrsim$0$''\!.$08 FWHM, it appears that for J_{AB} $\gtrsim$25 mag (B $\gtrsim$27 mag) both HST and the JWST may be more affected by natural confusion than by the traditional SB-limits. We suggest that this may already be visible in the deepest HDF images. This does however not mean that the deepest JWST samples will be fundamentally limited by natural confusion. Instead, we expect that for J_{AB} $\gtrsim$28–30 mag, the faint objects seen by JWST will be largely point sources at 0$''\!.$08 FWHM, which we begin to address here with hierarchical simulations using the models of Kawata (2001a, 200b). The first results of these simulations are shown as squares in Fig. 4. The good agreement between the black simulated galaxies and the observed colored points in the HDF for B_J $\lesssim$28 mag gives us confidence that the few available simulations for J_{AB} $\gtrsim$26 may yield accurate galaxy sizes. Also shown is the approximate size-range and expected flux-range for objects of globular cluster-type mass around the epoch of reionization (z$\simeq$7).

It is noteworthy that the expected object sizes for AB$\gtrsim$28 mag in Fig. 4 are mostly below the JWST diffraction limit ($\simeq$0$''\!.$08 FWHM), which we intend to confirm with further hierarchical simulations. This is an issue of critical importance and its consequences are further discussed in §6. If most objects with AB$\gtrsim$28 mag are indeed unresolved by JWST, then the deepest JWST images will be only limited by the instrumental confusion limit (as determined by JWST's instrumental FWHM$\simeq$0$''\!.$08), which doesn't set in until around J_{AB} $\gtrsim$33.5 mag. In that case, the hierarchical formation of galaxies together with the effects of the cosmological constant Λ at z$\lesssim$0.8 (Cohen et al. 2002) conspire to just keep the deepest JWST surveys away from the natural confusion limit in Fig. 4. These are important considerations for the precise definition of the FWHM and the exact PSF-shape of the JWST, which are currently being finalized.

The natural confusion limits plotted in Fig. 3–4 are somewhat uncertain due to the unknown size distribution, and because it is unknown how far we can push overlapping galaxy images before we: (a) loose the ability to make complete and reliable faint object catalogs (e.g. Bertin & Arnouts 1996), and (b) measure accurate fluxes and structural properties of faint galaxies (e.g., Odewahn et al. 2002). To better model the natural confusion limit, we need to better measure and model the galaxy size distribution over a very large dynamic range in flux, i.e. we must know the size distribution over the entire range 10$\lesssim$AB$\lesssim$30 mag. In a sequel paper, we will therefore combine all available data and models over the *entire* range 10$\lesssim$AB$\lesssim$33 mag (Fig. 2–4), which will result in a more accurate measure for the JWST natural confusion limit.

5. THE NATURAL CONFUSION LIMIT FOR THE SQUARE KILOMETER ARRAY

The Square Kilometer Array (SKA) radio interferometer is expected to become reality in the next decade (Hopkins et al. 2000, Ekers 2000). It will contain one square km of collecting area, and may exist of several thousand small (6 m) dishes placed in a geometrically increasing spiral pattern, and will likely have about 50% of the dishes in an inner core of 50 km maximum baseline that is heavily weighted towards high redshift H-I studies, and an outer core of $\lesssim$50% of the dishes that are spread over maximum baselines of several 100 to several 1000 km. Its exact location and instrument and receiver, etc., design are as yet unknown, but will be determined in the next few years. The SKA will have will have unprecedented sensitivity and resolution at radio wavelengths in the regime of a few 100

MHz to many GHz. Its goals are to have 0.001–0.1″ FWHM, about 1° FOV, and to reach sensitivity at nanoJy levels (100 nJy at 5-sigma in 12-hrs, and a putative goal of 10 nJy in a "super-HDF-like" campaign of 1200 hrs).

Having set constraints to the JWST natural confusion limit, it is relatively straightforward to calculate it for the SKA at GHz frequencies, since the same population of faint irregular, peculiar and merging/star-forming objects that dominates the faint galaxy counts will likely dominate the radio source counts at nanoJansky levels. For such objects, their radio sizes are likely similar to, or at least not much larger than their optical–IR sizes. If so, the SKA will need to have better than 50–100 m.a.s. FWHM to resolve them and not run into the instrumental natural confusion limit at 100 nanoJy at 1.4 GHz.

Critical for the natural confusion limit study is the faint radio source size distribution. In Fig. 6 we show the differential source counts and in Fig. 7 the median radio source size as a function of $S_{1.4}$ radio flux, with data as summarized in Windhorst et al. (1993, 2000) and updated with recent surveys. In general, the median radio source sizes decline steadily with radio flux over nearly 6 orders of magnitude in radio flux. The VLA+MERLIN results in HDF (Fig. 7) suggest that the sizes may be leveling off around 1″ FWHM, but this may be due to the limited beam-size and point source sensitivity available in the deep radio surveys carried out thus far. The dotted line is the best power-law fit to all data below $S_{1.4} \simeq$10 Jy, which is arbitrarily extrapolated to $S_{1.4} \simeq$10 nanoJy.

The ratio of radio to optical–near-IR sizes of star-forming objects is close to unity at least at local redshifts (Deeg et al. 1997). While this may not be strictly true at very high redshifts, there is no a priori reason why the radio continuum (*i.e.*, synchrotron) emission should have been extended much further from the galaxy center than the optical–near-IR light, and therefore it is reasonable to assume that for faint star-forming objects the radio continuum sizes are to first order the same as the optical–near-IR sizes from the star-forming disk as seen by JWST. In Fig. 7, we will plot therefore at the faint end the box with putative sizes (as upper limit in sizes!), as estimated from the JWST discussion in §4 and Fig. 2–4. This box coincides with the power-law extrapolation of the radio sizes measured to 100μJy .

Fig. 7 then shows the natural confusion limit as expected for SKA. As in Fig. 2–4, it was computed from the integrated source surface density, which was derived from the radio source counts in Fig. 6. Fig. 7 tentatively shows that the SKA will not run into the natural confusion limit at 100 nanoJy at 1.4 GHz. At levels of $S_{1.4} \simeq$10 nanoJy, the SKA will reach similar object surface densities as the JWST at $J_{AB} \simeq$33 mag (several to tens of 10^6 objects deg^{-2}). Like the JWST, the SKA may not run into the natural confusion limit at $S_{1.4} \simeq$10 nanoJy, *if* the slope of the nanoJy source counts remains below $\gamma \lesssim$1.7 (i.e., a magnitude slope $\alpha \lesssim$0.28), and *if* the ratio of radio to optical–near-IR sizes is similar at nanoJy levels.

6. DISCUSSION AND CONCLUSION

The natural confusion limit in ultradeep surveys must be carefully addressed. The following are our conclusions, and future work will need to consider the following issues:

• (1) The JWST diffraction limit should be kept around 0.″08–0.″10 FWHM, and its optics should be kept as close to diffraction-limited as possible at the shortest wavelengths (0.6–2μm), to mitigate the effects from natural confusion in ultradeep surveys at the faintest flux levels ($J_{AB} \gtrsim$28–32 mag).

• (2) If most objects at $J_{AB} \gtrsim$26–28 mag are indeed largely unresolved at the 0.″08 FWHM of JWST, as our few simulations available in Fig. 4 thus far suggest, then SB-sensitivity is not the overriding factor in designing ultradeep surveys, but point source sensitivity and natural confusion will be. This sword cuts on two sides. If objects with at $J_{AB} \gtrsim$28-30 mag are largely unresolved, then their structure and morphology will be harder to measure with JWST. However, if indeed largely unresolved, they will not suffer the full cosmological $\propto$(1+z)^4 SB-dimming, but instead their bolometric fluxes will only dim as $\propto$(1+z)^2, which makes them easier to detect, even at very high redshifts in deep JWST surveys.

• (3) SKA will need 0.01–0.05″ FWHM or better to resolve the faintest expected objects at large redshifts, i.e., objects of globular cluster-type mass or somewhat heavier that started shining around the epoch of reionization ($z_{ion} \simeq$6.5–7; Becker et al. 2001; Fig. 4 here). That is, to probe the "Epoch of First Light", SKA will need trans-continental sized baselines at 1.4 GHz (800-4000 km). Dynamic range and point-source sensitivity is critical for the SKA, but SB-sensitivity at scales$\gtrsim$0.3″ may not be as important for faint continuum objects at least. SKA will then be able to measure sizes for very small objects ($r_e \simeq$0.″01), which would require a D$\gtrsim$60 meter telescope in space at near-IR wavelengths. However, at nanoJy levels, JWST will likely detect such objects well before SKA can detect them at $S_{1.4} \simeq$10 nJy.

For both radio and optical surveys at nanoJy levels, we conclude that, counter to expectations, surface-brightness sensitivity may not be as important as the best possible resolution and point-source sensitivity for FWHM$\simeq$0.″08. The caveat here, of course, is that for larger objects at more intermediate redshifts (z$\lesssim$1 or $r_e \lesssim$0.″5–1.″0), SB-sensitivity is of utmost importance, so that telescopes like the SKA will have to be designed to have both excellent point-source sensitivity (at $\lesssim$0.″1 FWHM resolution) and excellent SB-sensitivity (at 0.″5–1.″0

FWHM). This is especially true because the fully two-dimensional spectroscopic capability of these future telescopes (i.e., redshifted H-I mapping for SKA and the MEMS-slitlets in NIRSpec for JWST) will allow us to spectrally disentangle objects at AB$\gtrsim$30 mag, even if they did spatially largely overlap.

• (4) To further predict the behavior of the natural confusion limit at AB$\gtrsim$28 mag before the JWST flies, one would need to do an ultradeep survey with the HST/ACS to I_{AB} $\simeq$31 mag. Better predictions about the expected nature of the faint object population and its role in the natural confusion limit will also come from more extensive hierarchical and/or semi-analytical models. These together can help us predict the size distribution of objects at AB$\simeq$28–36 mag, which will be of utmost importance when designing these ultradeep optical-IR—radio surveys of the future.

We thank Ron Ekers, Ray Norris and Lister Staveley-Smith for helpful discussions, and for hospitality at the ATNF during which part of this work was done. RAW, RAJ, SHC and SCO acknowledge funding for the HST part of this study from NASA grants GO.5985.01.94A, GO.6609.01.95A, AR.7534.02.96A from STScI, which is operated by AURA, Inc., under NASA contract NAS5-26555. We also acknowledge funding for the JWST part of this study from NASA Grant NAG5-12460. S. Cohen would like to thank the ASU NASA Space Grant Graduate Fellowship.

REFERENCES

Abraham, R. G., Tanvir, N.R., Santiago, B.X, Ellis, R.S., Glazebrook, K., van den Bergh, S. 1996, MNRAS, 279, L47

Becker, R. H., et al. 2001, AJ, 122, 2850

Benn, C. R., Grueff, G., Vigotti, M., & Wall J. V. 1982, MNRAS, 200, 747

Bertin, E., & Arnouts, S. 1996, AJ, 117, 393

Bruzual A., G. & Charlot, S. 1993, ApJ, 405, 538

Carlberg, R. G. 2002, ApJ, 573, 60

Cohen, S. H., Windhorst, R. A., Chiarenza, C. A. T., Odewahn, S. C., & Driver, S. P. 2002, AJ, submitted

Condon, J. J. 1974 , ApJ, 188, 279

Deeg, H.-J., Duric, N., Brinks, E. 1997, A&A, 323, 323

Driver, S. P., et al. 1998, ApJL, 496, L093 (astro-ph/9802092)

Driver, S. P., Windhorst, R. A., Ostrander, E. J., Keel, W. C., Griffiths, R. E., & Ratnatunga, K. U. 1995a, ApJL, 449, L023

Ekers, R. D. 2000, in "Looking Deep in the Southern Sky", Proceedings of the ESO/Australia Workshop, p. 146, Eds. F. Morganti and W. J. Couch (Berlin: Springer-Verlag)

Ellis, R. S. 1997, ARA&A, 35, 389 (astro-ph/9704019)

Fomalont, E. B., Partridge, R. B., Lowenthal, J. D., & Windhorst, R. A. 1993, ApJ, 404, 8

Fomalont, E. B., et al. 2002, AJ, 123, 2402 (astro-ph/0201441)

Gardner, J. P., & Satyapal, S. 2000, AJ, 119, 2589

Gardner, J. P. 1998, PASP, 110, 291

Glazebrook, K., Ellis, R. E. Santiago, B. & Griffiths, R. E. 1995b, MNRAS, 275, L19

Haiman, Z., & Loeb, A. 1998, ApJ, 519, 479

Hammer, F., Crampton, D., Lilly, S., LeFevre, O., Kenet, T. 1995, MNRAS, 276, 1085

Hogg, D. W. 2001, AJ, 121, 1207

Hopkins, A., Windhorst, R. A., Cram, L., & Ekers, R. 2000, Experimental Astronomy, Vol. 10, No. 4, 419 (astro-ph/9906469).

Hopkins, A., Afonso, J., Cram, L., Mobasher, B. 1999, ApJ, 519, L59

Im, M., & Stockman, H. S. 1999, in "Astrophysics with Infrared Surveys: A Prelude to SIRTF", ASP Conference Series, Vol. 177, p.75 Eds. Ed. M. D. Bicay, R. M. Cutri, and B. F. Madore. See also http://www.stsci.edu/ngst/science/simulations/im/

Kawata, D. 2001, ApJ, 558, 598 and — 2001, ApJ, 548, 703

Koo, D. C., & Kron, R. G. 1992, ARA&A, 30, 613;   Kron, R. G., Koo, D. C., & Windhorst, R. A. 1985, A&A, 146, 38

Liske, J. et al. 2002, MNRAS, submitted

Maihara, T. et al. 2001, PASJ, 53, 25

Marzke, R. O., Da Costa, L. N., Pellegrini, P. S., Willmer, C. N. A. & Geller, M. J. 1998, AJ, 503, 617

Mather, J. C., Stockman, H. S. 2000, Proc. SPIE Vol. 4013, p. 2-16, in "UV, Optical, and IR Space Telescopes and Instruments", Eds. J. B. Breckinridge & P. Jakobsen (Berlin: Springer)

Odewahn, S. C., Windhorst, R. A., Driver, S. P., & Keel, W. C. 1996, ApJL, 472, L013

Odewahn, S. C., Cohen, S. H., Windhorst, R. A., & Philip, N. S. 2002, ApJ, 568, 539 (astro-ph/0110275)

Petro, L. 2001, the Next Generation Space Telescope Simulator NMS, STScI, www.ngst.stsci.edu/nms/main/nms_flux_form.html

Richards, E. A. 2000, ApJ, 533, 611

Rieke, M. et al. 2002, Proc. SPIE Vol. xxxx, in press in "AstronomicalTelescopes and Instrumentation", Eds. R. Angel and J. B. Breckinridge (Berlin: Springer). See also http://ircamera.as.arizona.edu/nircam/

Scheuer, P. A. G. 1974, MNRAS, 166, 329

Stockman, H. S., Mather, J. C. 2000, in "The Extragalactic Infrared Background and its Cosmological Implications", IAU Symp. No. 204, p. 37 (Dordrecht: Kluwer)

Tyson, J. A. 1988, AJ, 96, 1

Windhorst, R. A., et al. B., Richards, E., Franklin, B. E., Pascarelle, S. M., & Griffiths, R. E. 1995, *Nature*, 375, 471

Windhorst, R. A., Fomalont, E. B., Partridge, R. B., & Lowenthal, J. D. 1993, ApJ, 405, 498

Windhorst, R. A., Miley, G. K., Owen, F. N., Kron, R. G., & Koo, D. C. 1985, ApJ, 289, 494

Windhorst, R. A., et al. 2000, in "The Hy-Redshift Universe: Galaxy Formation and Evolution at High Redshift", Eds. A. J. Bunker & W. J. M. van Breugel, ASP Conf. Ser. Vol. 193 (Provo, UT: Brigham Young University), p. 55

Fig. 1b. These are Figures 1 and 2 as reproduced from Gardner & Satyapal (2000) who summarized all available I-band counts, modeled these with the galaxy number count models of Gardner (1998), which included luminosity and SED evolution of the stellar populations and number density evolution due to reasonable merger scenarios, and then extrapolated these to fainter fluxes and longer wavelengths. At $\lambda \gtrsim 1\mu$m, the surface density at AB=34 can exceed 10^7 objects deg^{-2} , depending on the exact model used, which is an important consideration for the calculation of the natural confusion limit (see Figs. 3–6).

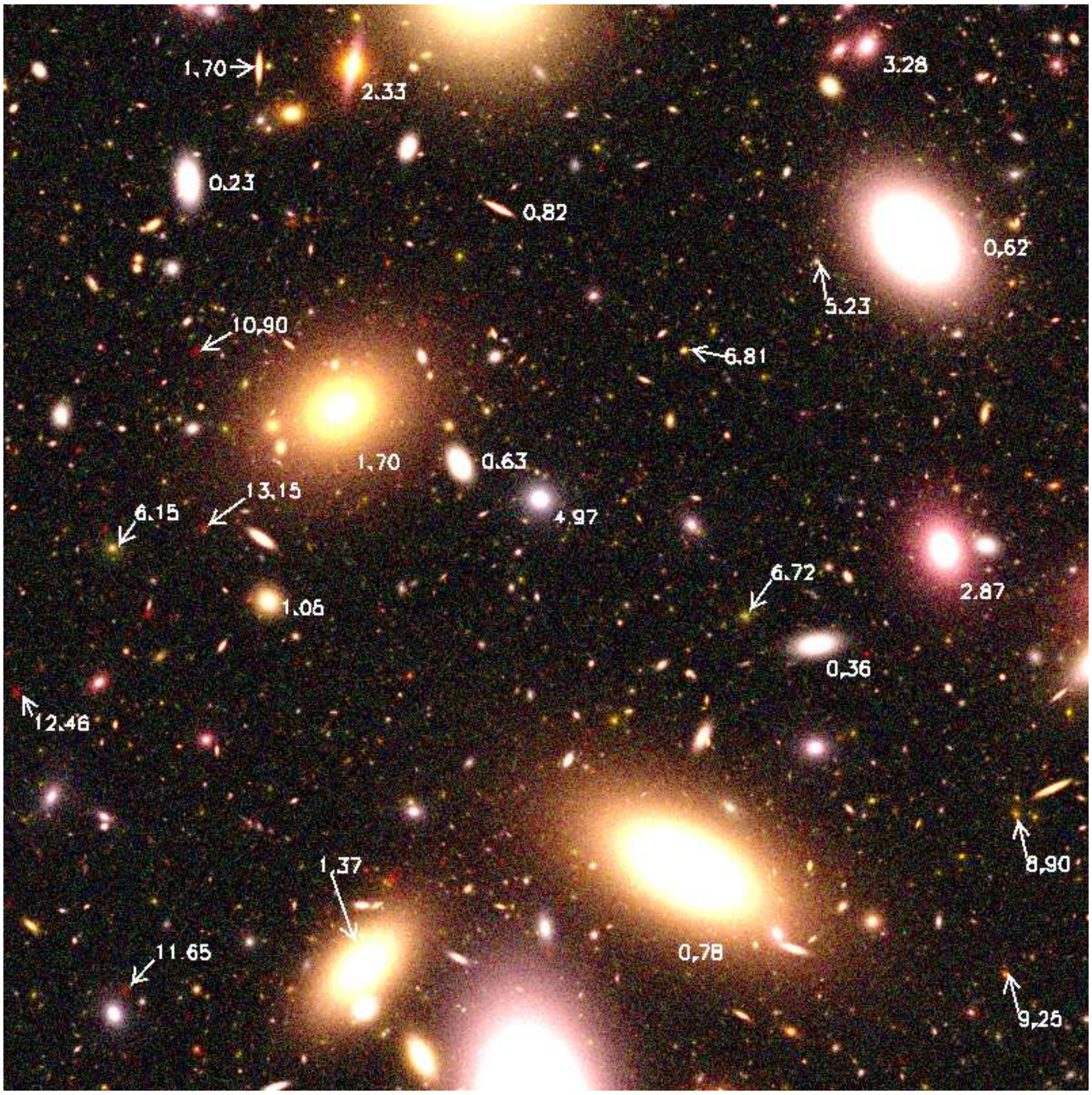

Fig. 1.— Simulation of a deep JWST image by Im and Stockman (1998), each having 18 hours of exposure in the I (0.8 micron), J (1.2 micron) and K (2.0 micron) filters with a relative bandwidth of 0.5. The images reach about AB=31.0 mag (10-σ) in each filter. Only $2{\times}2'$ of the NIRCam field of view is shown. A passive evolution was used to model the appearance of galaxies from z=0 to z=5, and the Press-Schechter formalism to model of star-forming proto-galaxies from z$\simeq$5 to z$\simeq$20 following Haiman and Loeb (1998). A few object redshifts are marked. Note that while individual object can be well distinguished, a small fraction of the objects begins to overlap due to their own small but finite object sizes (i.e. natural confusion). A statistical correction to the object counts and other studies requiring complete samples may have to be made for the effects of natural confusion (see Fig. 2–4).

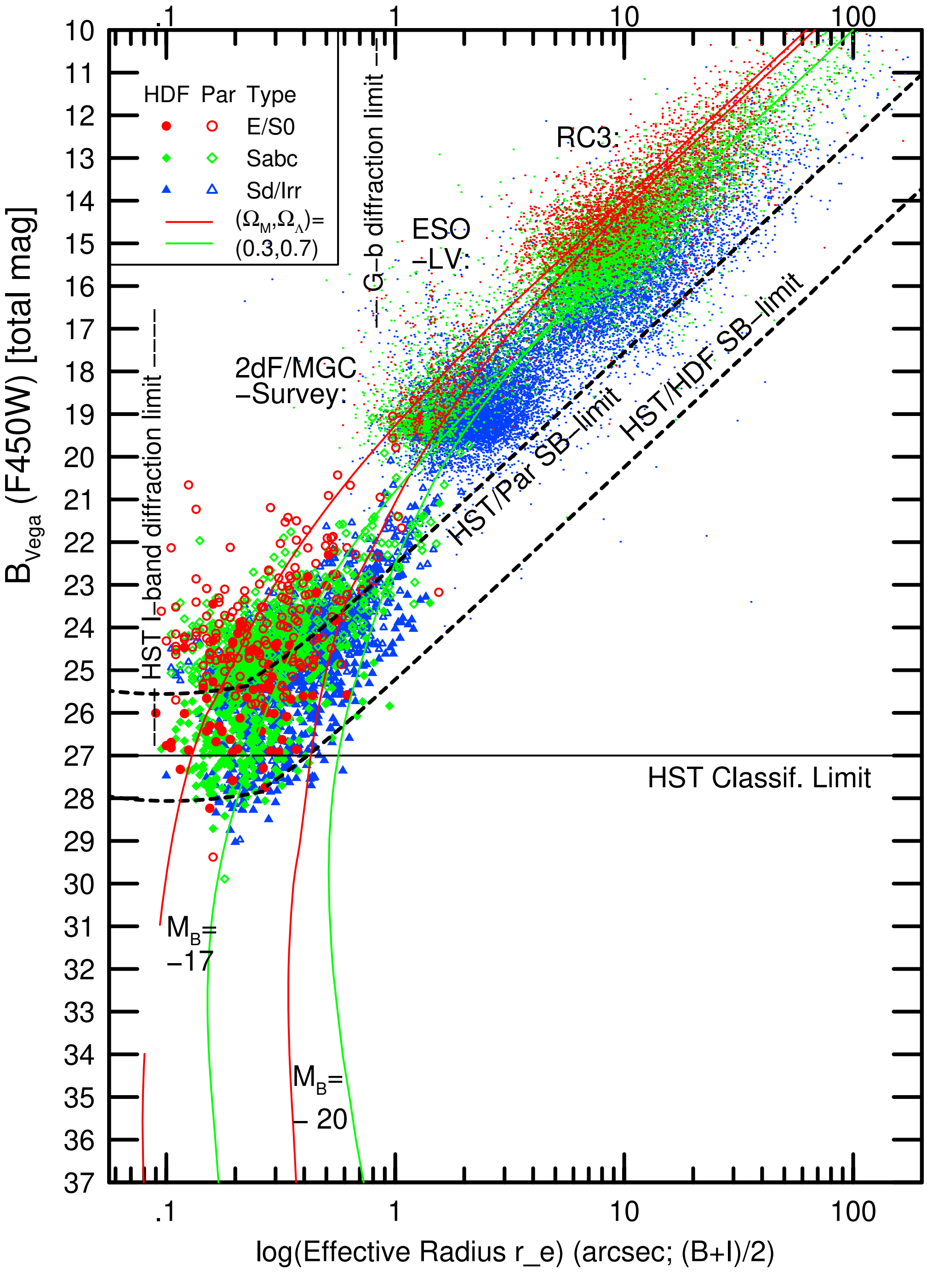

Fig. 2.— Summary of the relation between B–band flux (B_J -mag) and effective or half-light radius (r_e) for the entire galaxy population from the RC3 level to the HDF limit (B_J $\simeq$10–28 mag). Plotted are the ground-based RC3 and ESO Lauberts-Valentijn samples, which are both photographic surveys, but with good r_e measurements and galaxy types available, as well as the 2dF/MGC survey (Liske et al. 2002), which is a wide-area CCD survey with the 2.5 m INT telescope. At the faint end, the HST Parallel surveys are plotted, as well as three deep HST surveys including the two HDF's (Cohen et al. 2002, Odewahn et al. 1996). All fluxes are on the Vega B_J system (e.g., Kron 1980), since this is the only system currently publicly available with consistent data in the entire flux range AB$\simeq$10–28 mag. Symbols are color-coded according to ANN galaxy-type, as the legend indicates. The black dashed lines represent the point-source and SB-detection limits for Parallel and deep HST surveys, modeled through an exponential disk convolved with a Gaussian PSF (Cohen et al. 2002). *Note that the HDF data does not straddle the HST SB-limit well around* $r_e \simeq 1''$ *, which may be due to the onset of the natural confusion limit (see Fig. 4).* The red and green curves that are almost vertical at the faint end give the B_J $-r_e$ relations predicted from the type-dependent median sizes observed in the RC3 (which have median M_B $\simeq$–20 mag), redshifted for the cosmology in the legend. The black horizontal line at B_J $\simeq$27 mag indicates the HST classification limit. The M_B =–20 mag models show that most faint galaxies (of all types) are smaller than the median RC3 sizes, indicating the lower galaxy luminosities sampled at fainter fluxes, and suggesting the hierarchical growth of galaxy sizes with time.

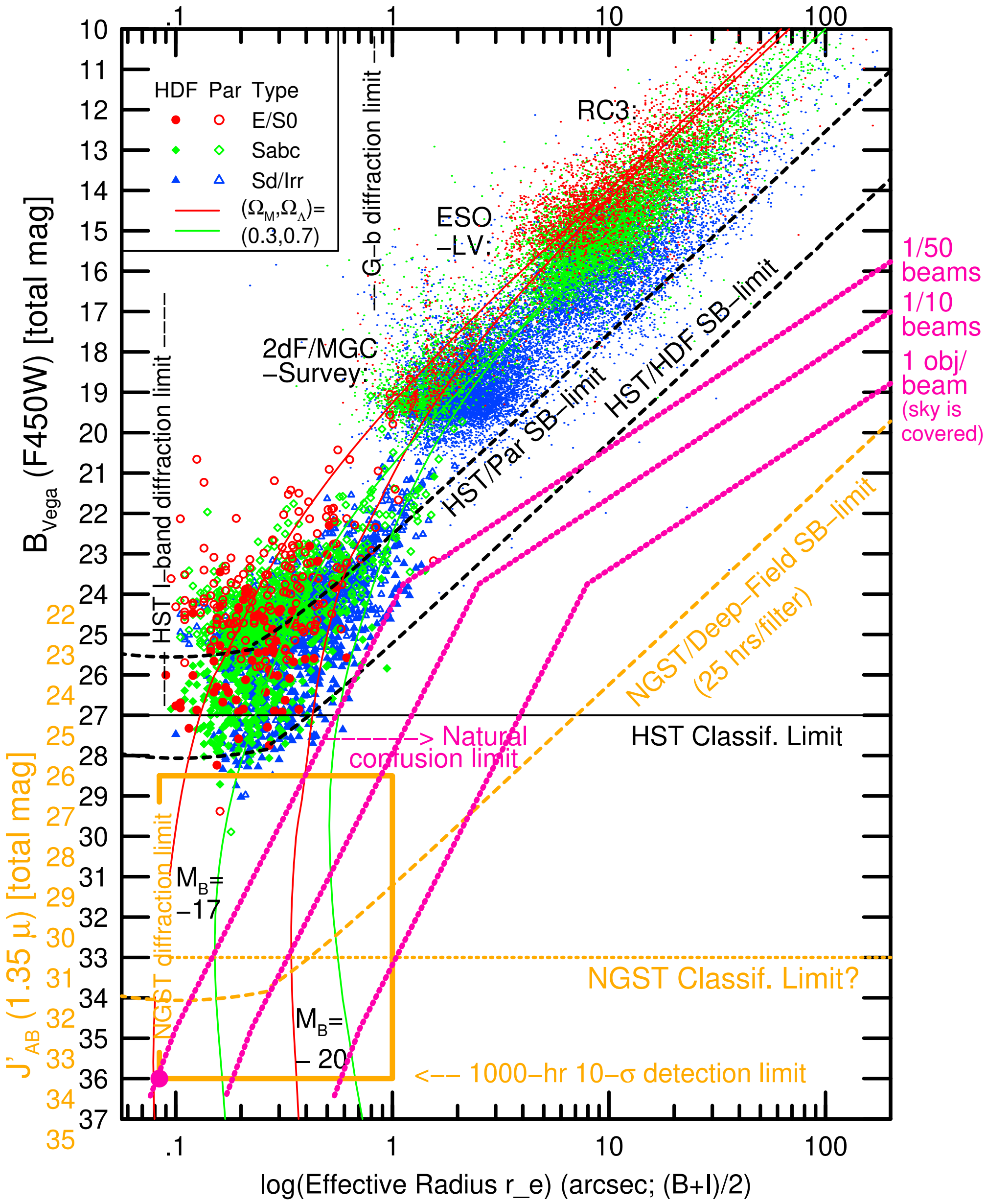

Fig. 3.— Same as in Fig. 2, but with the JWST sensitivity limits also plotted in orange, and with the natural confusion limits plotted in pink. For $B_J \gtrsim 28$ mag we adopt a J_{AB} flux scale, since JWST is not sensitive in the B_J -filter or anywhere below 0.6μm, and since the median redshift is expected to be $z_{med} \gtrsim 1$–2 (Driver et al. (1998) with a significant tail at z$\gtrsim$4, causing B-band drop-outs. For reasonable redshift distributions at AB$\gtrsim$28 mag ($z_{med} \simeq$2–4 and with a tail to $z_{max} \simeq z_{ion}$ $\simeq$7–10), J_{AB} -mags transform approximately to B_J -mag as indicated by the orange scale to the left. The J_{AB} point-source and SB-limit for a 25-hr JWST exposure are indicated by the curved orange dashed lines, and was computed as for the HST surveys in Fig. 2. The expected JWST classification limit is similarly indicated, although it is likely uncertain. Also indicated is the 10-σ J_{AB} point-source sensitivity limit for a 1000-hr "super-HDF-like" JWST campaign. The natural confusion limits are indicated by the three pink lines, which follow from *integrating* the I_{AB} galaxy counts in Fig. 1b (Gardner & Satyapal 2000), converted to J_{AB} using a Bruzual & Charlot (1993) model. The natural confusion lines are drawn for the level of 50 independent "beams" (or πr_e ^{2}'s) per detected object (i.e., the classical confusion limit, but now due to finite object sizes); at 10 independent "beams" per detected object; and at 1 "beam" per detected object, which is the level where the sky would be covered with half-light radii and started to look like a globular cluster. *Note that the HDF data does not straddle the HST SB-limit well around $r_e \simeq 1''$, which may indeed be due to natural confusion setting in around $B_J \simeq 24$ mag. This, however, would have only caused a relatively small fraction of the galaxies in the HDF being missed for $B_J \simeq 24$–28 mag by the SExtractor algorithm — see the discussion of blended objects by Williams et al. 1996).* The triangle bounded by the JWST diffraction limit (vertical orange line) and the slanted pink line for the 1/50 natural confusion limit is where most JWST objects are expected. Following the plotted models, these would have M_B =–17 mag or fainter. If all these faint JWST objects straddled the pink line, the deep JWST samples would be limited by natural confusion. However, we will argue in Fig. 4 that objects with $J_{AB} \gtrsim 28$ mag are likely mostly unresolved, and so they will instead straddle the JWST diffraction limit and skirt away from the 1/50 natural confusion limit line.

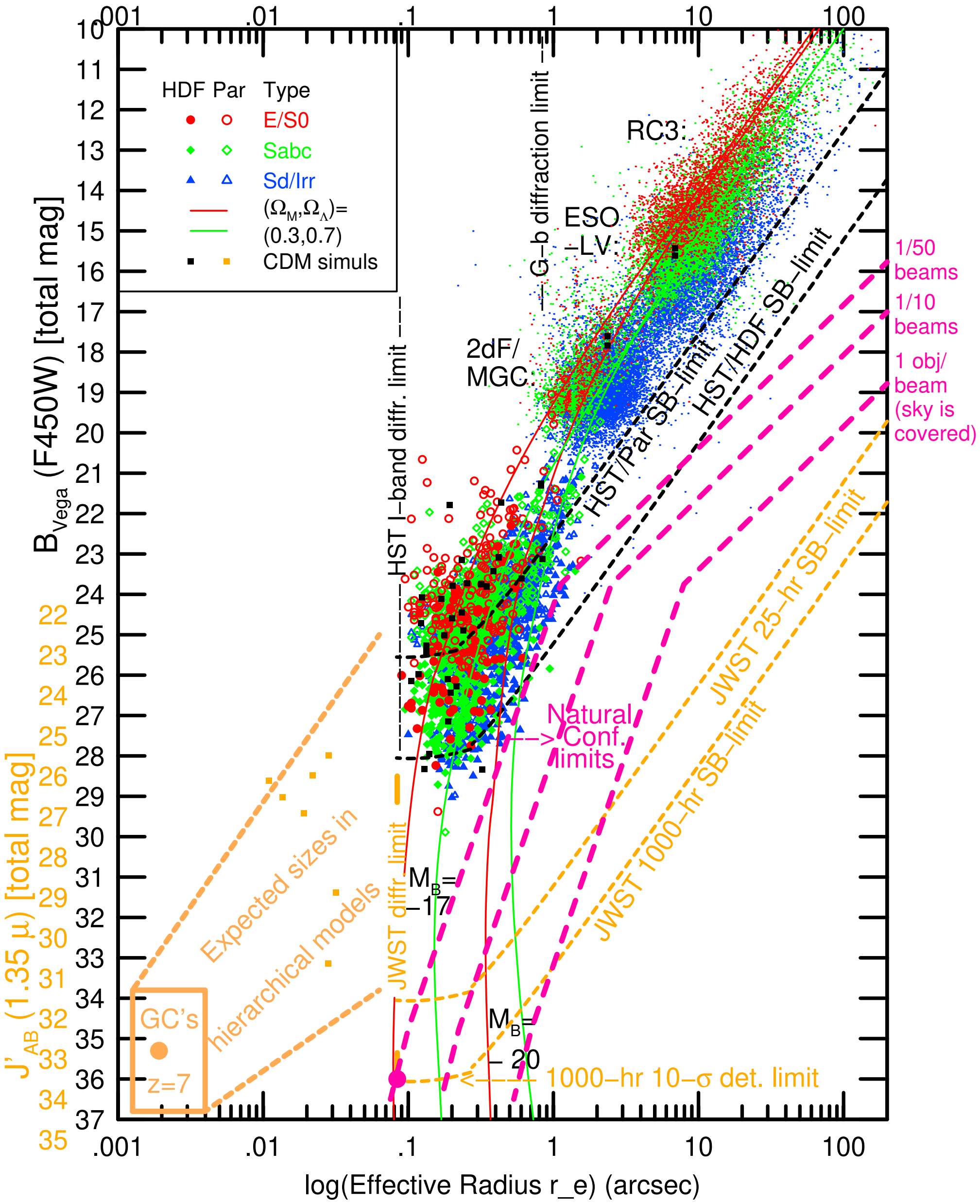

Fig. 4.— Same as in Fig. 2–3, but with the 100-hr JWST point-source and SB-sensitivity limits also plotted in orange, and the same natural confusion limits as in Fig. 3 in pink. The general area to the lower-right of the 1/50 and 1/10 natural confusion lines is not surveyable with sample completeness and reliability better than 98% and 90%, respectively. Our available hierarchical simulations using the models of Kawata (2001a, 200b) are plotted for $B_J \lesssim 28$ mag as black filled squares (using the B_J -mag scale, since most of these have simulated z$\lesssim$4). The good agreement between the black simulated galaxies and the observed colored points in the HDF for $B_J \lesssim 28$ mag gives us confidence that the few available simulations for $J_{AB} \gtrsim 26$ may yield accurate galaxy sizes. Also shown is the expected size-range and flux-range for objects of globular cluster-type mass around the epoch of reionization (z$\simeq$7). The expected object sizes in hierarchical models for $J_{AB} \gtrsim 26$–28 mag fall mostly below the JWST diffraction limit ($\simeq$0$''$.08 FWHM). If this is indeed true, then the deepest JWST images will be limited by the *instrumental* confusion limit (as determined by JWST's instrumental FWHM$\simeq$0$''$.08), which doesn't set in until $J_{AB} \gtrsim 33.5$ mag (big pink dot). In that case, the hierarchical formation of galaxies together with the effects of the cosmological constant Λ at z$\lesssim$0.8 (Cohen et al. 2002) conspire to just keep the deepest JWST surveys away from the natural confusion limit (pink lines). We plan on doing more hierarchical simulations of galaxy sizes with $J_{AB} \simeq$26–34 mag and $r_e \simeq$0$''$.001–0$''$.2 to confirm these findings. *Our most important conclusion is that deep JWST surveys for $J_{AB} \gtrsim 26$ mag, and even deep HST surveys for $B_J \gtrsim 24$ mag, start to become more limited by natural confusion than by the traditional SB-limitations. Yet, both are mostly limited by the point-source sensitivity of these telescopes. These findings must be further investigated by studying the behavior of object-finding algorithms on simulated images, as this issue will likely directly impact the technical specifications of future telescopes (e.g., the FWHM and the exact PSF-shape of the JWST and SKA), and the nature of future ultradeep surveys at nanoJansky levels.*

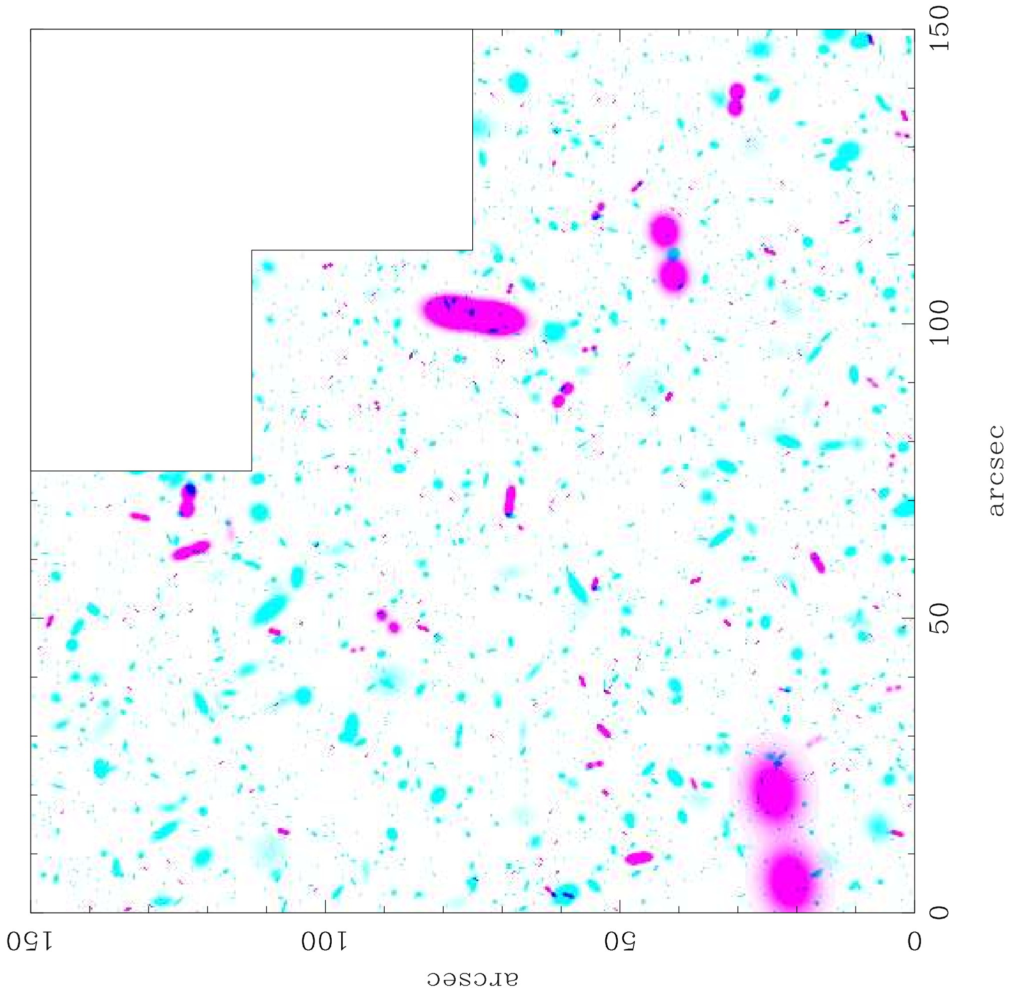

Fig. 5.— Simulated 1.4 GHz SKA image of Hopkins et al. (2000). This simulation includes the population of normal galaxies in addition to the IRAS-types. Details are given in the text and in Fig. 6. The FOV shape is that of the HST/WFPC2 and is $2\farcm5\times2\farcm5$ on a side. This SKA image has a simulated FWHM of $\simeq0\farcs1$ FWHM, and a flux density limit of 0.1 μJy (5-σ). There are 1941 objects in the simulation, 574 are AGN (red extended radio sources) and 1367 are star-formers (blue, mostly point-like or disk-shaped radio sources). Note that while individual radio sources can be well distinguished, a fraction of the objects begins to overlap due to their own small but finite object sizes (i.e. natural confusion). A statistical correction to the object counts and other studies requiring complete samples will have to be made for the effects of natural confusion. The real SKA may have maximum baselines well over 1000 km, and so FWHM$\lesssim0\farcs05$ at 1.4 GHz, which will help mitigate the effects from instrumental confusion, but not natural confusion (Fig. 3–4 and 7).

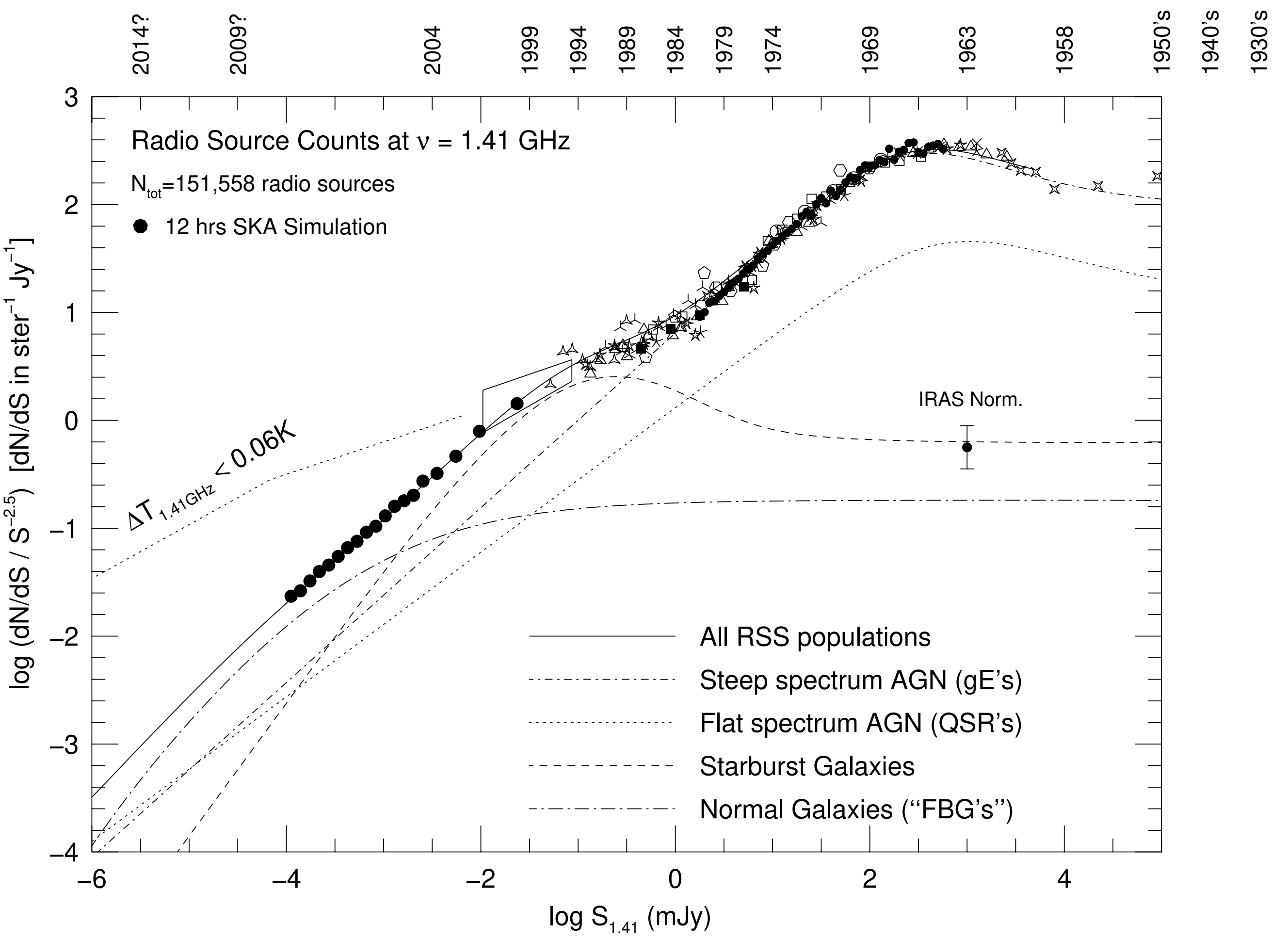

Fig. 6.— The observed normalized differential 1.41 GHz source counts. The various symbols are existing observed source counts, taken from surveys reviewed in Windhorst et al. (1993, 1999). Filled circles between 100 nJy–10μJy indicate a 12-hr simulation with the Square Kilometer Array (Hopkins et al. 2000). The straight dotted lines represents the upper limit to the nanoJy source counts from CBR temperature constraints (Fomalont et al. 1993, Windhorst et al. 1993). Models of the source counts are from Hopkins et al. (2000) as following: Dashed line: IRAS-type population; Dotted line: AGN flat-spectrum population ("Quasars"); Dot-dashed line: AGN steep-spectrum population ("Giant elliptical galaxies"); Dot-dash-dotted line: normal galaxy population; Solid line: sum of all populations. The maximum possible contribution is shown for the normal galaxy population (dot–long-dash). The extrapolation of the 1.4 GHz source counts below 10μJy is uncertain by at least 0.3 dex in the range 10–100 nJy (see Hopkins et al. 2000), depending on whether the high IRAS normalization is used for normal spirals, the standard normalization (as plotted here), or no normal spirals are added altogether.

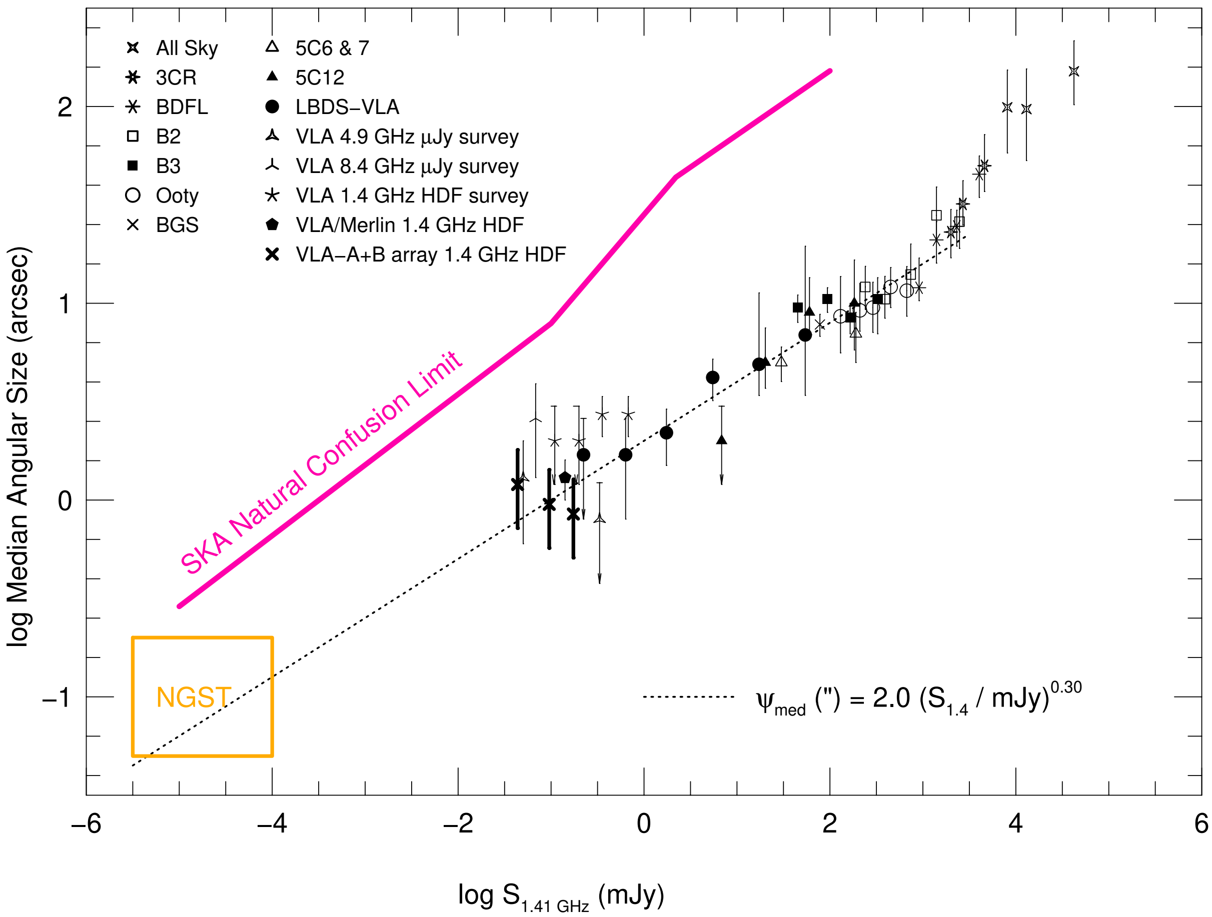

Fig. 7.— Median angular size vs. 1.41 GHz flux for low-frequency surveys, and for the deepest VLA surveys at 8.4, 4.86 and 1.4 GHz (Windhorst et al. 1993, Richards 1999, Fomalont et al. 2002). All flux scales were transformed to 1.41 GHz following the α_{med} vs S_{ν} relation of Windhorst et al. (2000). The dotted straight line is the best fit for $0.1 \lesssim S_{1.4} \lesssim 3000$ mJy, and was arbitrarily extrapolated as a straight power-law to 10 nanoJy. This extrapolation meets with the median JWST sizes expected at nanoJy levels, where both the extrapolated 1.4 GHz radio counts and the JWST object counts reach surface densities of several to tens of million per deg^2 . This suggests, although does not prove, that the expected SKA source sizes at 10–100 nanoJy may be <<0.″1. Hence, if the faintest radio emitting objects seen by SKA are also dominated by faint hierarchical growing objects as expected for JWST (Fig. 2–4), then the SKA will likely also remain below the natural confusion limit, provided that its longest baselines are several 1000 km at 1.4 GHz, so that its resolution is (much) better than 0.″05 FWHM (see Fig. 2–4).

Fig. 2. Summary of the relation between B–band flux (B_J -mag) and effective or half-light radius (r_e) for the entire galaxy population from the RC3 level to the HDF limit ($B_J \simeq$10–28 mag). Plotted are the ground-based RC3 and ESO Lauberts-Valentijn samples, which are both photographic surveys, but with good r_e measurements and galaxy types available, as well as the 2dF/MGC survey (Liske et al. 2002), which is a wide-area CCD survey with the 2.5 m INT telescope. At the faint end, the HST Parallel surveys are plotted, as well as three deep HST surveys including the two HDF's (Cohen et al. 2002, Odewahn et al. 1996). All fluxes are on the Vega B_J system (e.g., Kron 1980), since this is the only system currently publicly available with consistent data in the entire flux range AB$\simeq$10–28 mag. Symbols are color-coded according to ANN galaxy-type, as the legend indicates. The black dashed lines represent the point-source and SB-detection limits for Parallel and deep HST surveys, modeled through an exponential disk convolved with a Gaussian PSF (Cohen et al. 2002). *Note that the HDF data does not straddle the HST SB-limit well around* $r_e \simeq 1''$ *, which may be due to the onset of the natural confusion limit (see Fig. 4).* The red and green curves that are almost vertical at the faint end give the B_J –r_e relations predicted from the type-dependent median sizes observed in the RC3 (which have median $M_B \simeq$–20 mag), redshifted for the cosmology in the legend. The black horizontal line at $B_J \simeq$27 mag indicates the HST classification limit. The M_B =–20 mag models show that most faint galaxies (of all types) are smaller than the median RC3 sizes, indicating the lower galaxy luminosities sampled at fainter fluxes, and suggesting the hierarchical growth of galaxy sizes with time.

Fig. 3. Same as in Fig. 2, but with the JWST sensitivity limits also plotted in orange, and with the natural confusion limits plotted in pink. For $B_J \gtrsim 28$ mag we adopt a J_{AB} flux scale, since JWST is not sensitive in the B_J -filter or anywhere below 0.6μm, and since the median redshift is expected to be $z_{med} \gtrsim 1$–2 (Driver et al. (1998) with a significant tail at z$\gtrsim$4, causing B-band drop-outs. For reasonable redshift distributions at AB$\gtrsim$28 mag ($z_{med} \simeq 2$–4 and with a tail to $z_{max} \simeq z_{ion} \simeq 7$–10), J_{AB} -mags transform approximately to B_J -mag as indicated by the orange scale to the left. The J_{AB} point-source and SB-limit for a 25-hr JWST exposure are indicated by the curved orange dashed lines, and was computed as for the HST surveys in Fig. 2. The expected JWST classification limit is similarly indicated, although it is likely uncertain. Also indicated is the 10-σ J_{AB} point-source sensitivity limit for a 1000-hr "super-HDF-like" JWST campaign. The natural confusion limits are indicated by the three pink lines, which follow from *integrating* the I_{AB} galaxy counts in Fig. 1b (Gardner & Satyapal 2000), converted to J_{AB} using a Bruzual & Charlot (1993) model. The natural confusion lines are drawn for the level of 50 independent "beams" (or $\pi r_e{}^2$'s) per detected object (i.e., the classical confusion limit, but now due to finite object sizes); at 10 independent "beams" per detected object; and at 1 "beam" per detected object, which is the level where the sky would be covered with half-light radii and started to look like a globular cluster. *Note that the HDF data does not straddle the HST SB-limit well around $r_e \simeq 1''$, which may indeed be due to natural confusion setting in around $B_J \simeq 24$ mag. This, however, would have only caused a relatively small fraction of the galaxies in the HDF being missed for $B_J \simeq 24$–28 mag by the SExtractor algorithm — see the discussion of blended objects by Williams et al. 1996).* The triangle bounded by the JWST diffraction limit (vertical orange line) and the slanted pink line for the 1/50 natural confusion limit is where most JWST objects are expected. Following the plotted models, these would have $M_B = -17$ mag or fainter. If all these faint JWST objects straddled the pink line, the deep JWST samples would be limited by natural confusion. However, we will argue in Fig. 4 that objects with $J_{AB} \gtrsim 28$ mag are likely mostly unresolved, and so they will instead straddle the JWST diffraction limit and skirt away from the 1/50 natural confusion limit line.

Fig. 4. Same as in Fig. 2–3, but with the 100-hr JWST point-source and SB-sensitivity limits also plotted in orange, and the same natural confusion limits as in Fig. 3 in pink. The general area to the lower-right of the 1/50 and 1/10 natural confusion lines is not surveyable with sample completeness and reliability better than 98% and 90%, respectively. Our available hierarchical simulations using the models of Kawata (2001a, 200b) are plotted for $B_J \lesssim 28$ mag as black filled squares (using the B_J -mag scale, since most of these have simulated z$\lesssim$4). The good agreement between the black simulated galaxies and the observed colored points in the HDF for $B_J \lesssim 28$ mag gives us confidence that the few available simulations for $J_{AB} \gtrsim 26$ may yield accurate galaxy sizes. Also shown is the expected size-range and flux-range for objects of globular cluster-type mass around the epoch of reionization (z$\simeq$7). The expected object sizes in hierarchical models for $J_{AB} \gtrsim 26$–28 mag fall mostly below the JWST diffraction limit ($\simeq$0$''$.08 FWHM). If this is indeed true, then the deepest JWST images will be limited by the *instrumental* confusion limit (as determined by JWST's instrumental FWHM$\simeq$0$''$.08), which doesn't set in until $J_{AB} \gtrsim 33.5$ mag (big pink dot). In that case, the hierarchical formation of galaxies together with the effects of the cosmological constant Λ at z$\lesssim$0.8 (Cohen et al. 2002) conspire to just keep the deepest JWST surveys away from the natural confusion limit (pink lines). We plan on doing more hierarchical simulations of galaxy sizes with $J_{AB} \simeq$26–34 mag and $r_e \simeq$0$''$.001–0$''$.2 to confirm these findings. *Our most important conclusion is that deep JWST surveys for $J_{AB} \gtrsim 26$ mag, and even deep HST surveys for $B_J \gtrsim 24$ mag, start to become more limited by natural confusion than by the traditional SB-limitations. Yet, both are mostly limited by the point-source sensitivity of these telescopes. These findings must be further investigated by studying the behavior of object-finding algorithms on simulated images, as this issue will likely directly impact the technical specifications of future telescopes (e.g., the FWHM and the exact PSF-shape of the JWST and SKA), and the nature of future ultradeep surveys at nanoJansky levels.*